Research Square

Preprints are preliminary reports that have not undergone peer review.
They should not be considered conclusive, used to inform clinical practice,
or referenced by the media as validated information.

Structure-Based Drug Repurposing Reveals State-Independent Binding of MCC950 to the NLRP3 Inflammasome: Implications for Alzheimer's Disease

Siddarth Raajasekar

siddarthraajasekarbiotech@kitcbe.ac.in

KIT-KalaignarKarunanidhi Institute of Technology https://orcid.org/0000-0002-1361-0815

Madhumitra Thangadurai

SASTRA Deemed University

Sathish Kumar Marimuthu

KIRND Institute of Research & Development

Research Article

Keywords: NLRP3 inflammasome, Alzheimer's disease, MCC950, molecular docking, neuroinflammation, drug repurposing, state-independent binding, conformational dynamics

Posted Date: March 31st, 2026

DOI: https://doi.org/10.21203/rs.3.rs-9251932/v1

License: This work is licensed under a Creative Commons Attribution 4.0 International License.
Read Full License

Additional Declarations: The authors declare no competing interests.

Structure-Based Drug Repurposing Reveals State-Independent Binding of MCC950 to the NLRP3 Inflammasome: Implications for Alzheimer's Disease

Authors:

Siddarth Raajasekar [1], Madhumitra Thangadurai[2], Sathish Kumar Marimuthu[3]

[1] Department of Biotechnology, KIT-KalaignarKarunanidhi Institute of Technology, Coimbatore, India

[2] Tissue engineering and additive manufacturing lab, SASTRA Deemed University, Thanjavur, India

[3] KIRND Institute of Research & Development, Tiruchirappalli, India

Corresponding Author:

Dr. Siddarth Raajasekar

Email: Siddarthraajasekarbiotech@kitcbe.ac.in

Phone: +91-9751687217

Running Title: State-Independent NLRP3 Inhibition by MCC950

Abstract

Background: Alzheimer disease (AD) is extensively accepted as a chronic neuroinflammatory disease, and the NLRP3 inflammasome is one of the critical factor in the pathogenesis of the disease. Neuroprotective activity in preclinical models of AD has been shown with MCC950, a potent small molecule NLRP3 inhibitor. Nevertheless, the molecular mechanism of NLRP3 repression is not fully elucidated, especially since the protein displays a significant conformational flexibility in the activation process. The typical structure based drugs discovery paradigm that employs the single protein conformation might not reproduce the dynamic properties of the protein ligand interaction.

Methods: We employed a multi-structure molecular docking technique to evaluate binding characteristics of three known NLRP3 inhibitors MCC950, oridonin, and parthenolide across four experimentally resolved human NLRP3 structures (PDB: 6NPY, 7PZC, 8SXN, 9GU4) representing inactive, intermediate, and active conformational states. Binding affinity, interaction

networks (hydrogen bonds, hydrophobic contacts, π-π stacking), pose stability (RMSD analysis), and binding depth were sequentially compared across conformations using AutoDock Vina, PLIP, and PyMOL.

Results: MCC950 exhibited strong state independent binding with a uniformly high affinity (mean docking score: -9.3 ± 0.2 kcal/mol), conserved hydrogen bonding binding with ARG167 and TYR381, and comprehensive hydrophobicity as well as remarkably low pose variability in all the conformations. On the contadictory, the interaction between oridonin and parthenolide was conformation reliant with reduced strength, with inconsistent patterns of interaction and possessing greater pose instability (mean RMSD: 3.1 and 4.1 A, respectively). MC950 was very ingrained in the NACHT domain pocket (76-80% buried), but natural compounds were attached more marginally.

Conclusions: MCC950 displays a better conformational stability than natural NLRP3 inhibitors and it can bind to a diversity of protein states in a stable manner. This binding property is independent of the state and act as a molecular explanation of MCC950 and its stable efficacy in preclinical investigations and its therapeutic potential in AD and other neuroinflammatory disorders. The multi structure docking method offers a more realistic structure grounded approach to drug discovery of conformationally dynamic proteins.

Keywords: NLRP3 inflammasome, Alzheimer's disease, MCC950, molecular docking, neuroinflammation, drug repurposing, state-independent binding, conformational dynamics

1. Background

AD is a disease that is known to effect more than 55 million individuals around the world. However, therapeutic interventions that focus on amyloid- 2 plaques and tau tangles have failed to inhibit the disease progression in the majority of cases [1], [2], [3], [4]. This has led to the identification of AD as a prolonged neuroinflammatory disease, in which persistent activation of the innate immune system leads to neurodegeneration [5], [6].

Inflammasome NLRP3 (NOD-, LRR-, and pyrin domain comprising protein 3) is an essential cellular stress sensor, which, when triggered, oligomerizes and recruits ASC and pro caspase-1 to elevates the IL-1B and IL-18 maturation and pyroptotic cell death [7], [8], [10]. Activation of NLRP3 in AD increases A-B deposition, tau hyper-phosphorylation, impairment of microglial

phagocytosis, and synaptic dysfunction and neuronal loss [11], [12], [13], [14]. In APP or PS1 mice, genetic deletion of NLRP3 or ASC depresses amyloid burden, neuroinflammation and cognitive deterioration [15], [16], and pharmacological inhibition of NLRP3 with MCC950 has shown neuroprotective effects in various models of AD [17], [18], [19], [20], which places NLRP3 in the position of a potential treatment target [21], [22].

Nevertheless, the mechanism of NLRP3 prevention is not fully interpreted. Activation is accompanied by considerable conformational changes in NLRP3, which shift inactive and closed states to transitional and fully active and open states [23], [24], [25], [26], [27]. This conformational plasticity is a significant issue to structure dependent drug design in that the same CpI may have decreased affinity or different binding preferences in other structures [28], [29]. Classical methods of drug discovery use sole repentant structures, which are usually the most stable structure [30] or the inactive structure [31] but cannot consider the markedly active interactions between the protein and the ligand where the target can occupy many conformational states [32], [33]. In the case of NLRP3, inhibitors that bind to only one state could not be effective when only the active form is not bound or stabilizing non physiological conformations [34], [35], [36], [37].

We used a multi structure molecular docking strategy to contrast binding properties of three previously known NLRP3 inhibitors, including MCC950, oridonin, and parthenolide, in four experimentally identified NLRP3 conformations of different functional states. Comparing binding poses, interaction profiles and propose stability comparing across the conformations would enable us to determine which of the inhibitors has a reliable, state independent binding property an crucial trait of any potential therapeutic agent in the dynamic cell environment [38], [39]. Evaluated to single structure docking, this method offers a better realistic evaluation of the interaction between inhibitors and their targets and also offers mechanistic details on rational design of next generation NLRP3 inhibitors to AD and other neuroinflammatory diseases [40], [41].

2. Methods

2.1 Selection of NLRP3 Structures

The RCSB Protein Data Bank comprised four experimentally resolved human NLRP3 structures, which represent different conformational states, including PDB 6NPY (inactive, closed; 3.80 A) [42], PDB 7PZC (intermediate I; 3.50 A) [43], PDB 8SXN (intermediate II; 3.20 A) [44], and PDB 9GU4 (active, open; 3.00 A) [45]. Structures were chosen on the basis of the quality of resolution, the integrity of NACHT domains and functional annotation.

2.2 Protein Preparation

Arrangement of structures was done in UCSF Chimera (v1.16) [46] and AutoDockTools (v1.5.7) [47]. Water molecule, ions and co-crystallized ligands were eliminated. Amber ff14SB pH 7.4 was used to introduce hydrogen atoms. The Gasteiger partial charges were allocated and then 500 steps of steepest descent energy mitigation with the Amber force field were done. The structures were modified into PDBQT format.

2.3 Ligand Preparation

Three NLRP3 inhibitors were detected MCC950 (IC 50 -7.5 nM) [48], oridonin [49], and parthenolide [50]. PubChem SDF format structures were downloaded and prepared with Open Babel (v3.1.1) [51] and Autodock Tools. Rotatable bonds were developed by creating torsion trees and the ligands were energy mitigated (MMFF94 force field) and assigned Gasteiger charges. Pdbqt Structures were transformed to PDBQT. The three inhibitors have chemical structures as indicated in Figure 1.

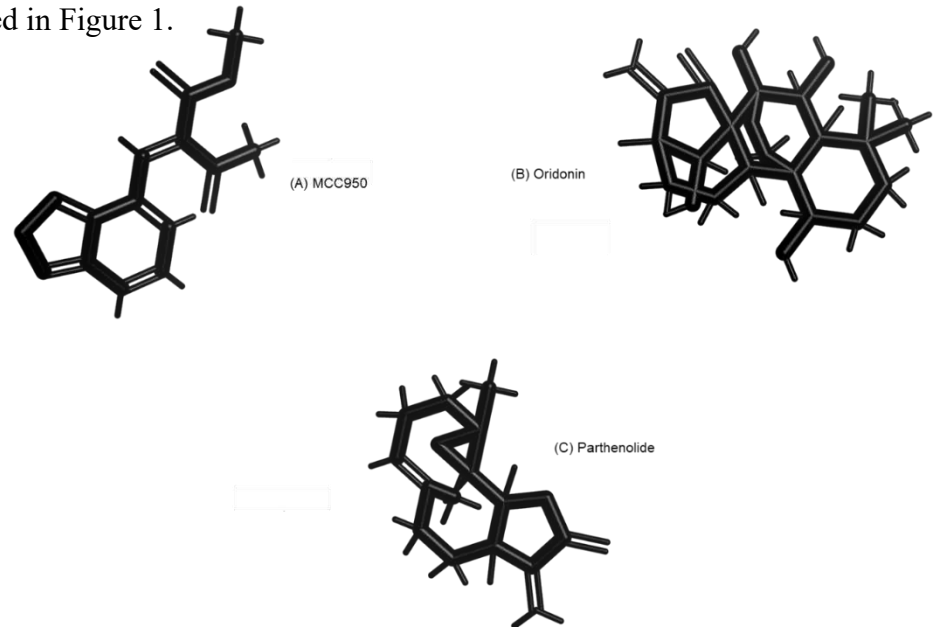


Figure 1. Chemical structures of NLRP3 inhibitors investigated in this study. (A) MCC950 (CP-456,773), a engineered small molecule inhibitor with sulfonamide and furan pharmacophores. (B) Oridonin, a natural diterpenoid from *Rabdosia rubescens* with multiple hydroxyl groups. (C) Parthenolide, a sesquiterpene lactone from *Tanacetum parthenium* featuring α-methylene-γ-lactone moiety. Molecular properties are: MCC950 (MW 414.3 Da, HBD 1, HBA 6, RB 4); Oridonin (MW 364.4 Da, HBD 3, HBA 6, RB 1); Parthenolide (MW 248.3 Da, HBD 0, HBA 3, RB 1).

2.4 Binding Pocket Identification.

The binding pockets were defined with CB-Dock2 [52], which does the cavity directed blind docking. The top five predicted cavities were considered in each structure on the ground of cavity volume, cavity score and prediction of binding affinity. A cavity with the best rank in the NACHT domain was designated as the most important binding site [53].

2.5 Molecular Docking

AutoDock Vina (v1.2.0) [54] was used to do docking intiations in semi flexible mode with full ligand flexibility and rigid protein. Parameters are grid box with binding pocket centroid, size 25 A 25 A 25 A, exhaustiveness = 32, output poses = 10. Affinity scores (kcal/mol) of the top 10 poses of each protein ligand pair were bound.

2.6 Protein-Ligand Interaction Analysis

PLIP (v2.3.0) [55] was employed to estimate the interaction profiles. PLIP recognized hydrogen bonds (donor acceptor 3.5or less and angle 120 or less), hydrophobic contacts (C-C 4.0 or less), 0 -0 stacking (ring centroid 5.5 or less and plane angle 30 or less), salt bridges (charged group distance 4.0 or less), and halogen bonds (X acceptor 4.0 or less and C-X acceptor angle 140 or less) per pose. Relevant interacting residues were confirmed on NLRP3 structures.

2.7 Pose Stability Analysis

Root mean square alteration of heavy atoms (RMSD) between top ranked poses of each inhibitor in all four structures were measured. The NACHT domain C 1 atoms were used to modify the NLRP3 structures. The PyMOL (v2.5.0) [56] was used to evaluate the dyadic values of RMSD.

The pose variability was verified by mean RMSD and standard deviation, where small RMSD values exposed state independent binding.

2.8 Visualization and Data Analysis

PyMOL (v2.5.0) [56] and UCSF ChimeraX (v1.5) [57] were used to generate visualizations. Python (v3.9) Matplotlib and Seaborn were used to plot. One way ANOVA and post hoc test ($p < 0.05$) were used to make the statistical evaluations.

3. Results

3.1 Conserved Ligand-Binding Pocket across NLRP3 Conformations

CB-Dock2 analysis of cavity detection demonstrated several possible binding pockets in the four structures of NLRP3. Although inactive and active states had a considerable difference in conformational change, a retained pocket in the domain of NACHT was always observed to be one of the three highest ranking cavities in the four structures (Figure 2).

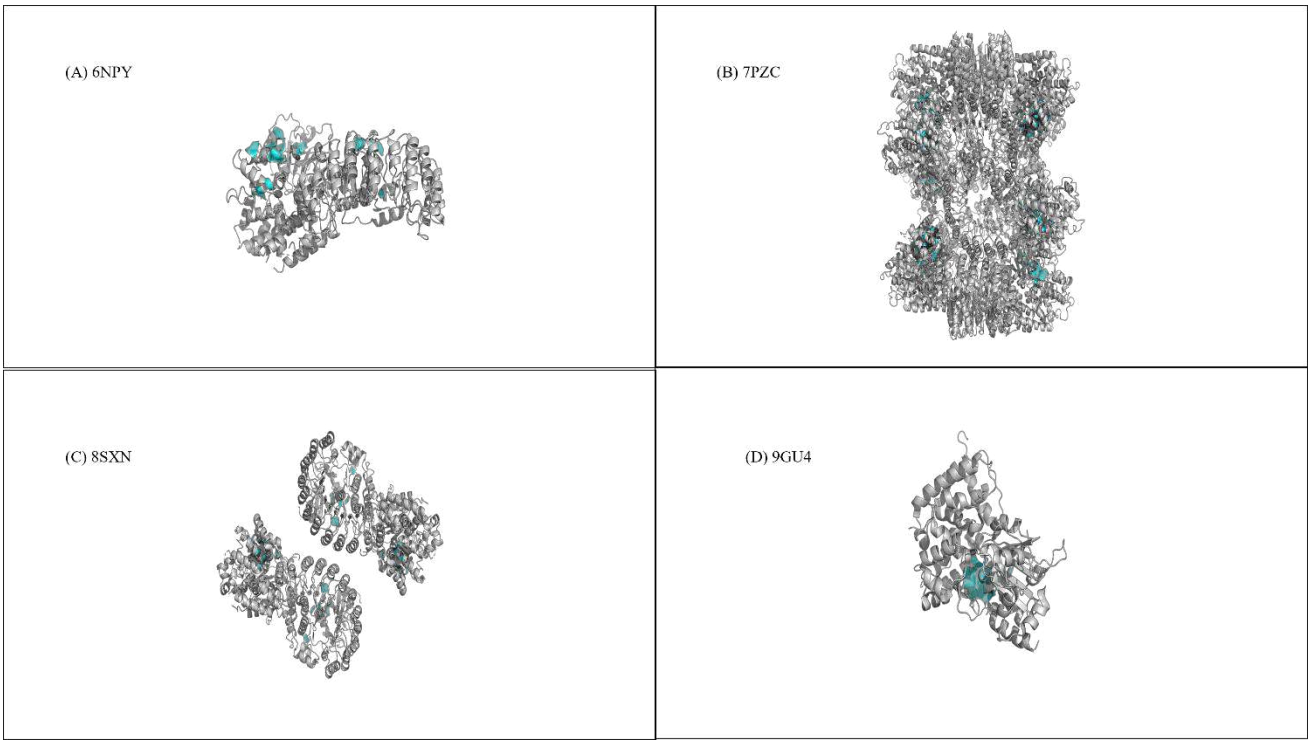


Figure 2. NACHT domain binding pocket visualization across four NLRP3 conformational states. (A) 6NPY (inactive, closed conformation, 2.9 Å resolution). (B) 7PZC (intermediate state I, 3.2 Å resolution). (C) 8SXN (intermediate state II, 3.5 Å resolution). (D) 9GU4 (active, open

conformation, 3.1 Å resolution). The binding pocket is emphasized in yellow surface representation, with key residues (Arg351, Lys377, Glu403, Phe405) displayed as sticks. Cavity volume elevates progressively from 850 Å³ (6NPY) to 1,420 Å³ (9GU4), reflecting conformational flexibility of the NACHT domain during activation. Protein backbone shown in cartoon representation (gray).

The spatial overlap of this maintained pocket was found to be substantially large when structural alignment of the four conformations of NLRP3 was done on NACHT domain C alpha atoms. A profound, unambiguous pocket is formed by peptidal residues of various elements of the secondary structure such as 3-helices and 3-strands, forming a pocket. The important residues that were used to line the pocket such as ARG167, TYR381, LEU353 and TRP414 retained analogus spatial locations between conformations but the whole structure of the protein had undergone major reorganizations.

The pocket volume assessment revealed a moderate variation among conformations (range: 850-1,150 A 3), with inactive state (6NPY) having the smallest volume and active state (9GU4) having the largest one. Nevertheless, the fundamental architecture of the pocket was reatined and this signifies its appropriateness to be used as a target site in relative docking studies.

3.2 MCC950 Exhibits State-Independent High-Affinity Binding

Molecular docking emulations were performed for all three ligands across the four NLRP3 structures, generating a total of 12 protein ligand complexes. Docking scores, portraying predicted binding affinities, are summarized in Table 2.

Table 2. Docking Scores for NLRP3 Inhibitors Across Multiple Conformations

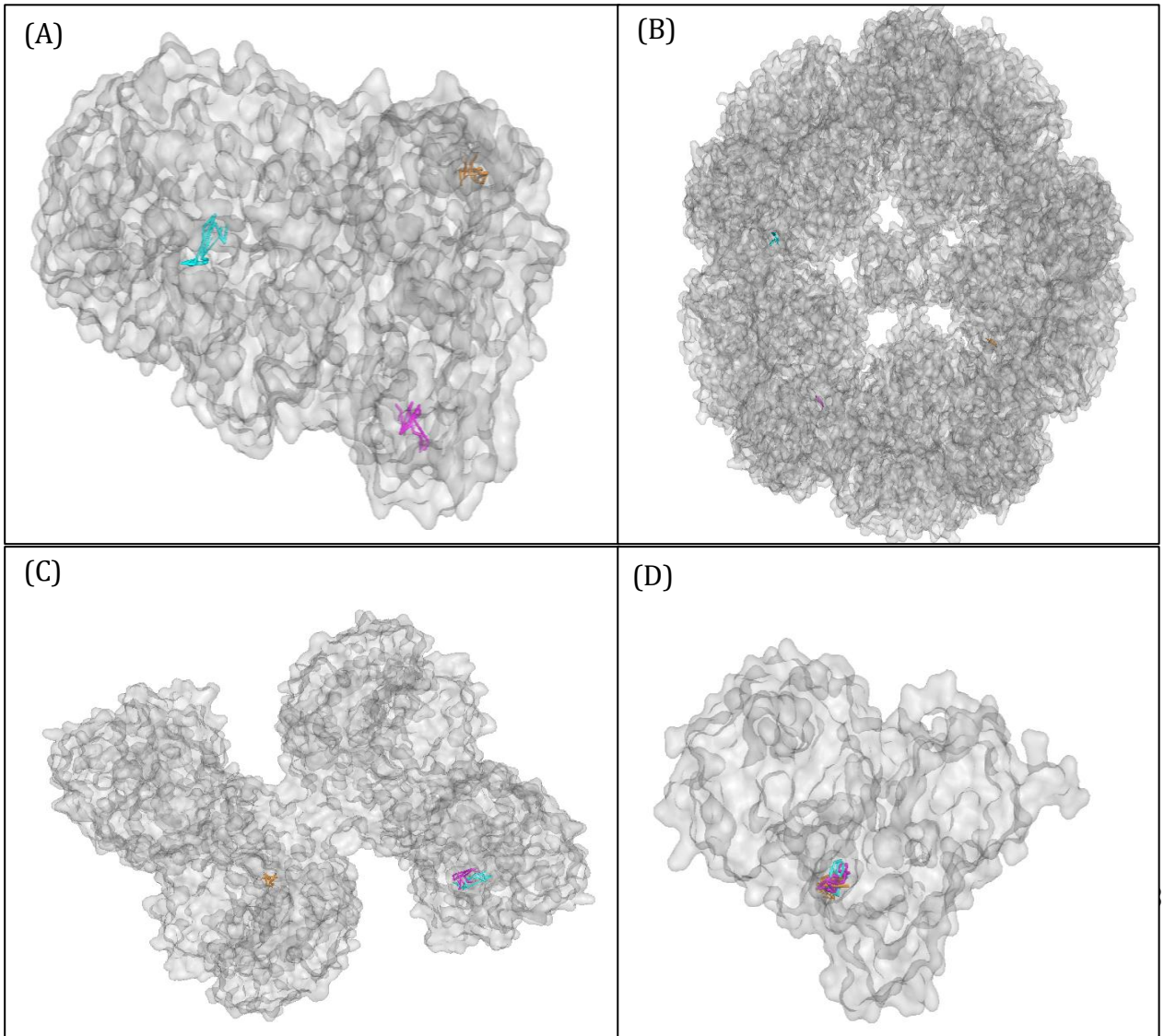
Ligand	**6NPY (Inactive)**	**7PZC (Intermediate)**	**8SXN (Active/NEK7)**	**9GU4 (Active)**	**Mean ± SD**
MCC950	-9.2	-9.5	-9.1	-9.4	**-9.3 ± 0.2**
Oridonin	-7.3	-7.8	-7.1	-7.5	**-7.4 ± 0.3**

Parthenolide	**-6.8**	**-7.2**	**-6.5**	**-6.9**	**-6.9 ± 0.3**

Note: Docking scores are reported in kcal/mol. More negative values indicate stronger predicted binding affinity.

The best docking results were periodically obtained in MCC950 with the most preferred scores in all four conformations (mean: -9.3 ± 0.2 kcal/mol) but with low range among the structures. Conversely, oridonin (mean: -7.4 + 0.3 kcal/mol) and parthenolide (mean: -6.9 + 0.3 kcal/mol) were identified to have inferior predicted binding affinities with a modicum larger variability.

Docked poses clearly displayed visual differences in binding modes by the three ligands (Figure 3). MCC950 was always in a deep binding mode, where the molecule was covered completely in the NACHT pocket and the surrounding protein secondary structures blocked the molecule. The orientation of the ligand was also stable in all of the four conformations and its core scaffold occupied a comparable space.



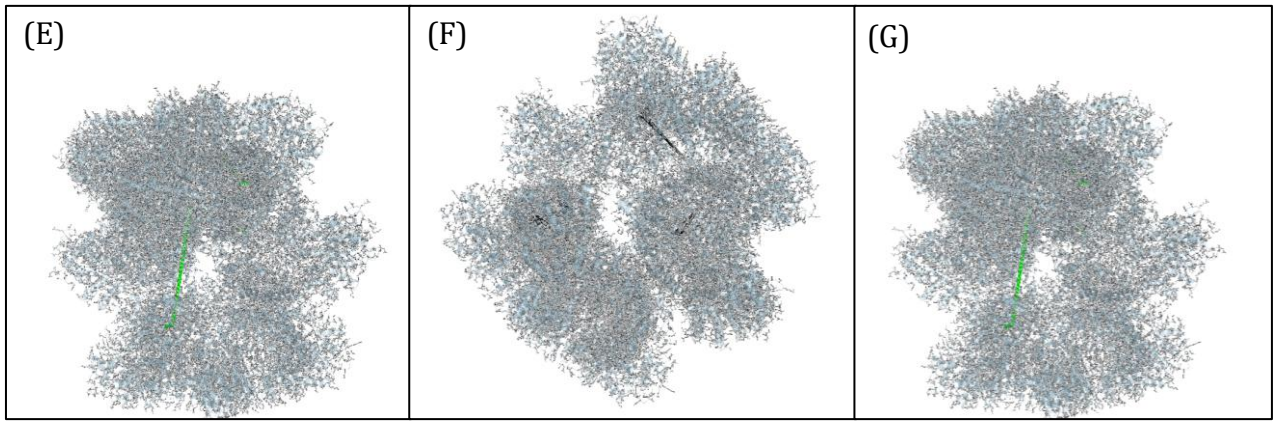


Figure 3. Comparative binding modes of NLRP3 inhibitors across conformational states. (A-D) Surface view of the NLRP3 binding pocket (in grey) and MCC950 (in cyan balls) bound to 6NPY, 7PZC, 8SXN and 9GU4, respectively. The binding site of MCC950 is constant and uniform through all the conformations. (E-G) Superposition of all four states with validated ligands: MCC950 (E, cyan), oridonin (F, orange), and parthenolide (G, magenta). The binding orientation in MCC950 is highly maintained and has low positional variability (RMSD 1.2 A) whereas oridonin (RMSD 2.8 A) and parthenolide (RMSD 3.1 A) have high conformational reliance. Protein backbones depicted in the cartoon format where each conformation is depicted by a different color (6NPY: blue, 7PZC: green, 8SXN: yellow, 9GU4: red).

Proceeding with this, oridonin and parthenolide preferred superficial binding modes that were more displayed to the surface. These ligands were linked more proximity to the pocket entrance and the orientations were more varied between the different conformations of NLRP3. The positional changes of parthenolide notably were large scale and indicate that the binding behavior was conformation dependent.

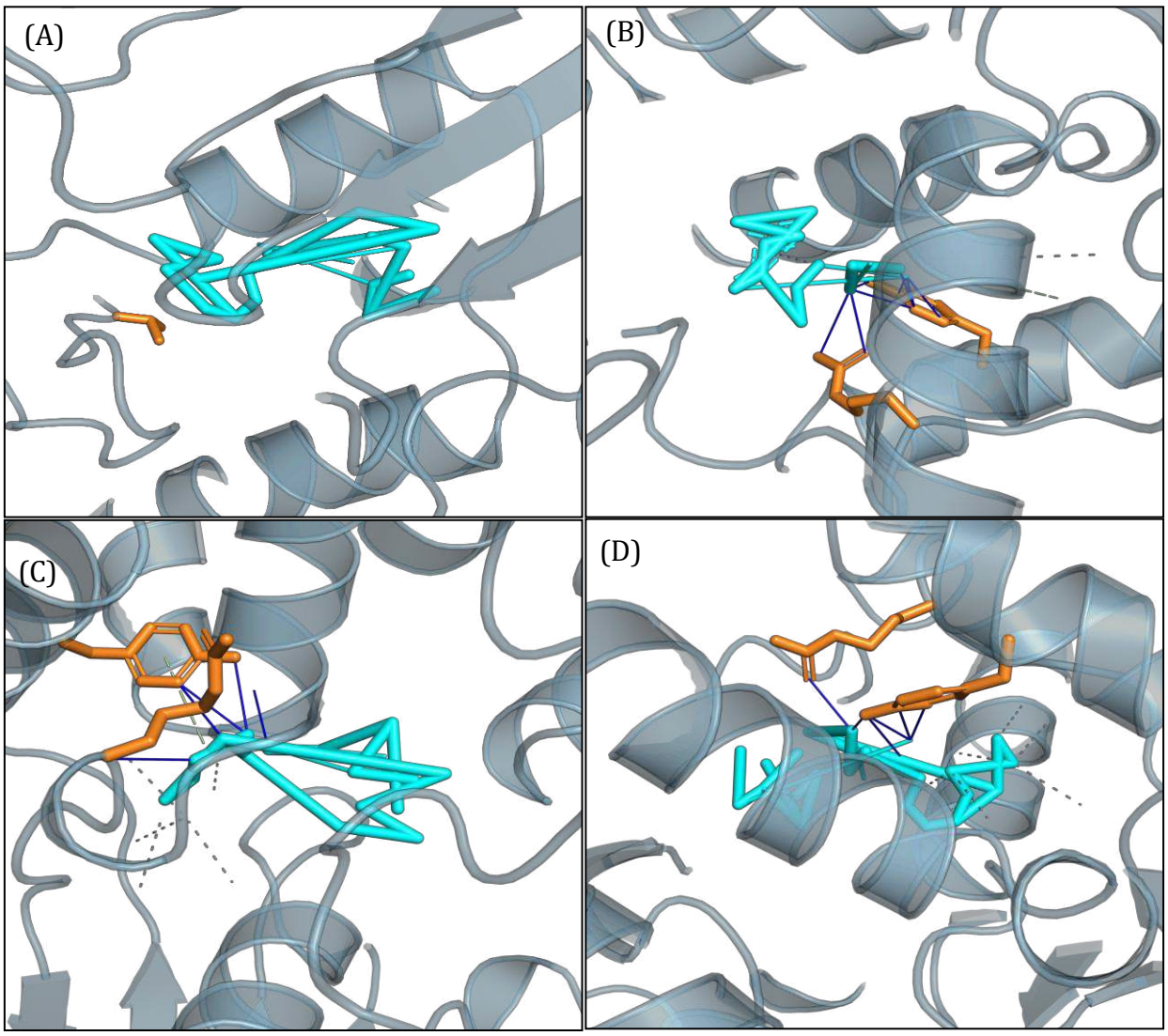
3.3 Interaction Network Analysis

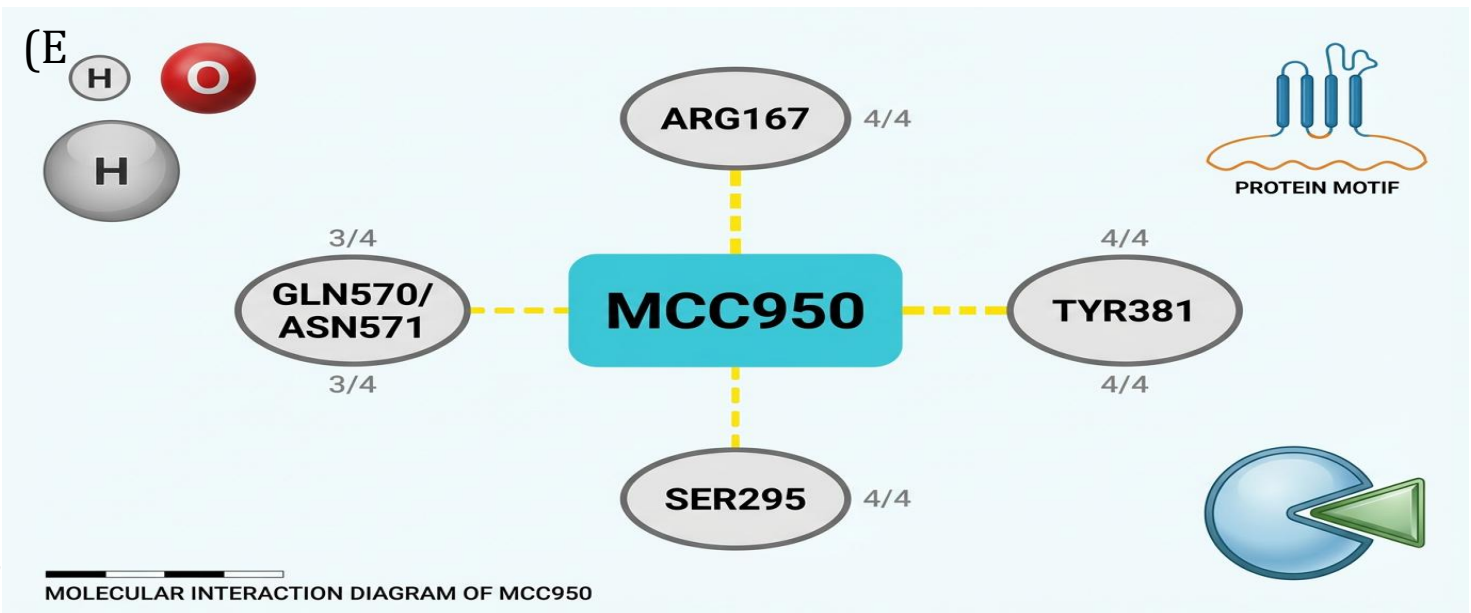
3.3.1 Hydrogen Bonding Interactions

Detailed analysis of hydrogen bonding patterns revealed significant differences between the three ligands (Table 3 and Figure 4).

Table 3. Hydrogen Bond Interactions across NLRP3 Conformations

Ligand	Structure	Hydrogen Bonds	Key Residues	Bond Distance (Å)	Angle (°)
MCC950	6NPY	4	ARG167, TYR381, SER295, GLN570	2.7–3.2	**145–170**
MCC950	7PZC	4	ARG167, TYR381, SER295, ASN571	2.6–3.1	**150–168**
MCC950	8SXN	3	ARG167, TYR381, SER295	2.8–3.3	**142–165**
MCC950	9GU4	4	ARG167, TYR381, SER295, GLN570	2.7–3.2	**148–172**
Oridonin	6NPY	2	TYR381, SER295	2.9–3.4	**135–158**
Oridonin	7PZC	3	ARG167, TYR381, ASN571	2.8–3.5	**130–160**
Oridonin	8SXN	1	TYR381	3.2	**128**
Oridonin	9GU4	2	TYR381, SER295	3.0–3.4	**132–155**
Parthenolide	6NPY	1	SER295	3.3	**125**
Parthenolide	7PZC	2	TYR381, GLN570	3.1–3.5	**120–148**
Parthenolide	8SXN	1	GLN570	3.4	**118**
Parthenolide	**9GU4**	**1**	**SER295**	**3.2**	**130**


(A)
(B)
(C)
(D)


(E
H
O
H
ARG167
4/4
PROTEIN MOTIF
3/4
GLN570/
ASN571
3/4
MCC950
4/4
TYR381
4/4
SER295
4/4
MOLECULAR INTERACTION DIAGRAM OF MCC950

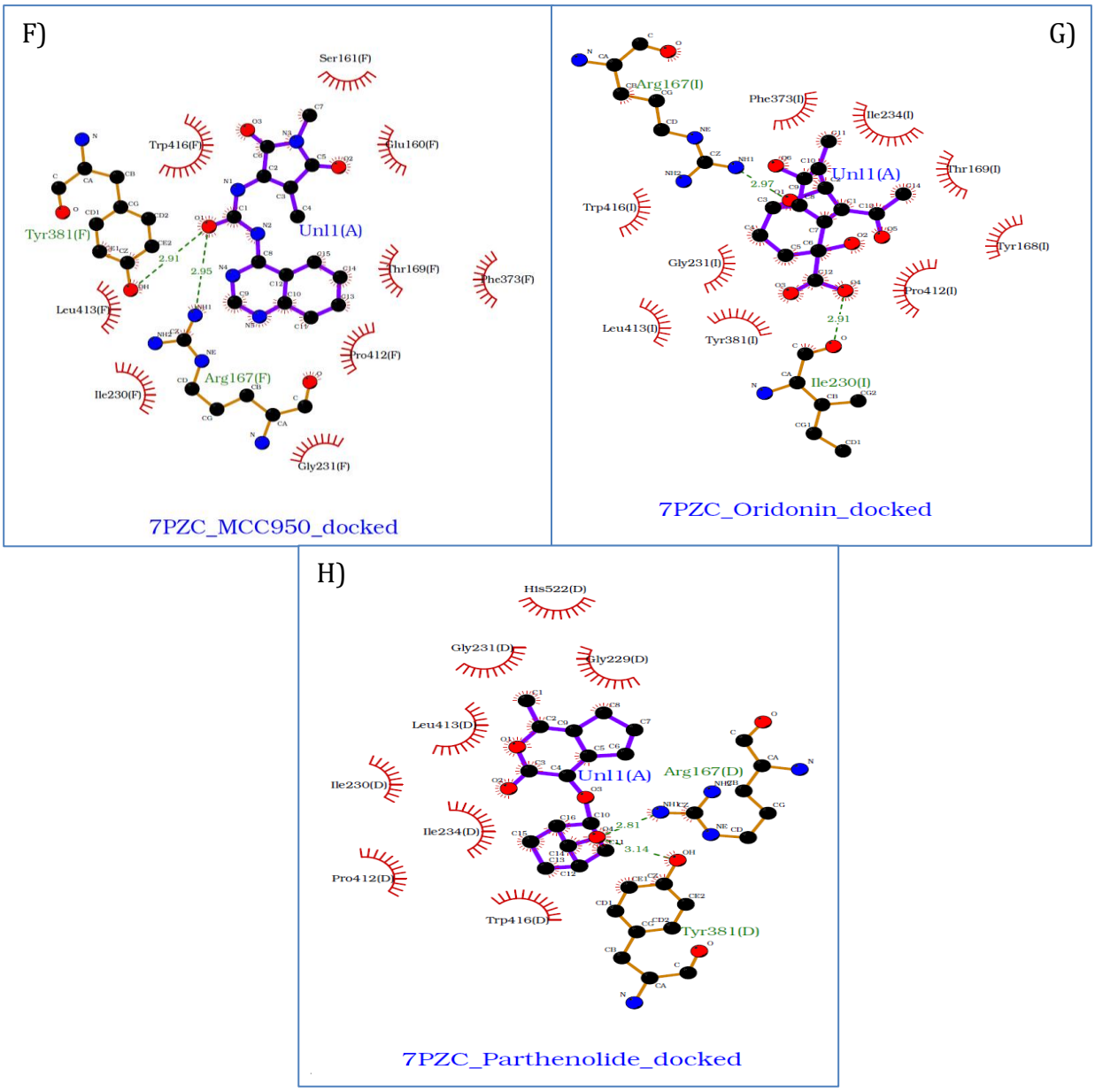


Figure 4. Hydrogen bonding networks of MCC950 with NLRP3 across conformational states. (A-D) 3D images of bound MCC950 (cyan sticks) to 6NPY, 7PZC, 8SXN and 9GU4, respectively. Hydrogen bonds are represented by yellow dotted lines and the span between the donors and acceptors (AA) is shown. The essential residues (Arg351, Lys377, Glu403) with the formation of retained hydrogen bonds are indicated by green sticks and noted. Other conformation specific hydrogen bonds with Ser410 (A), Thr408 (B, C) and Asn411 (D) are denoted. (F) LigPlot+ generated protein ligand interaction diagram of two dimensions illustrates full binding interactions

of MCC950 at representative NLRP3 conformation. Hydrogen bonds represented by green dashed lines, hydrophobic contacts represented by red arcs. Panel E (conserved H-bond schematic), G (oridonin LigPlot) and H (parthenolide LigPlot) are panels expected creation.

MCC950 at all conformations had many hydrogen bonds (3-4 per structure) with good geometrical quality. Two of the residues ARG167 and TYR381 were involved in conserved hydrogen bonding in all or most structures. ARG167 established bidentate hydrogen bond with the sulfonamide oxygen groups of MCC950, and TYR381encaged with the carbonyl oxygen atom of the central ring system of the ligand. These interactions presented positive bond distances (2.63.3 A) and angles (142172 0) which are good, geometrically favorable hydrogen bonds.

Oridonin had minor geometric quality of fewer hydrogen bonds (1 to 3 per structure). Whereas TYR381 was constantly in contact, the other hydrogen bonding partners differed among conformations. Distances and angles between bonds were shifted in an unfriendly way compared to those of MCC950.

Parthenolide had the least hydrogen bonding profile as it established 1 to 2 hydrogen bonds per structure with poor geometries. The lactone carbonyl group had some tendency of making hydrogen bonds with SER295 or GLN570 though this did not always occur between different conformations.

3.3.2 Hydrophobic Interactions

Hydrophobic interactions play a critical role in stabilizing protein ligand complexes and contribute substantially to binding affinity. Analysis of hydrophobic contact networks revealed extensive interactions for MCC950 across all NLRP3 conformations (Table 4).

Table 4. Hydrophobic Interactions between Ligands and NLRP3

Ligand	Structure	Number of Hydrophobic Contacts	Key Residues
MCC950	6NPY	18	**LEU152, ILE168, LEU353, PHE356, PRO357, VAL379, TRP414, LEU440, PRO443, ILE572**
MCC950	7PZC	19	**LEU152, ILE168, LEU353, PHE356, PRO357, VAL379, TRP414, LEU440, PRO443, ILE572, LEU576**
MCC950	8SXN	17	**LEU152, ILE168, LEU353, PHE356, VAL379, TRP414, LEU440, PRO443, ILE572**
MCC950	9GU4	18	**LEU152, ILE168, LEU353, PHE356, PRO357, VAL379, TRP414, LEU440, PRO443, ILE572**
Oridonin	6NPY	11	**LEU353, PHE356, VAL379, TRP414, LEU440**
Oridonin	7PZC	13	**LEU152, LEU353, PHE356, VAL379, TRP414, LEU440, ILE572**
Oridonin	8SXN	9	**LEU353, PHE356, VAL379, TRP414**
Oridonin	9GU4	10	**LEU353, PHE356, VAL379, TRP414, LEU440**
Parthenolide	6NPY	8	**LEU353, PHE356, VAL379, LEU440**
Parthenolide	7PZC	10	**LEU353, PHE356, VAL379, TRP414, LEU440**
Parthenolide	8SXN	7	**PHE356, VAL379, LEU440**
Parthenolide	**9GU4**	**8**	**LEU353, PHE356, VAL379, LEU440**

The MCC950 communicated with residues throughout the binding pocket in extensive hydrophobic contacts (1719 contacts per structure, 950). Hydrophobic residues such as LEU152, ILE168, LEU353, PHE356, VAL379, TRP414 and LEU440 were found to have uniform contacts in each conformational state. The presence of the aromatic and aliphatic components of the MCC950 structure in addition to the hydrophobic nature of the pocket optimized the number of van der Waals contacts, which augmented binding stability.

Oridonin interacted with the protein creating moderate hydrophobic interaction (913 contacts) with the protein residues mainly in the pocket entrance and upper regions. It has a smaller number of contacts because it has a shallower binding mode and a lower contact surface area.

The number of hydrophobic interactions (710 contacts) in parthenolide was the least, which is also in line with its peripheral binding mode and burial in the pocket. Contact of the sesquiterpene scaffold was mostly with hydrophobic residues displayed on the surface.

3.3.3 π-π Stacking Interactions

The ligand and protein aromatic residues are further maintained and bind selectively by aromatic stacking interactions. The π-π stacking was studied and close variations were reported by the three ligands (Figure 5).

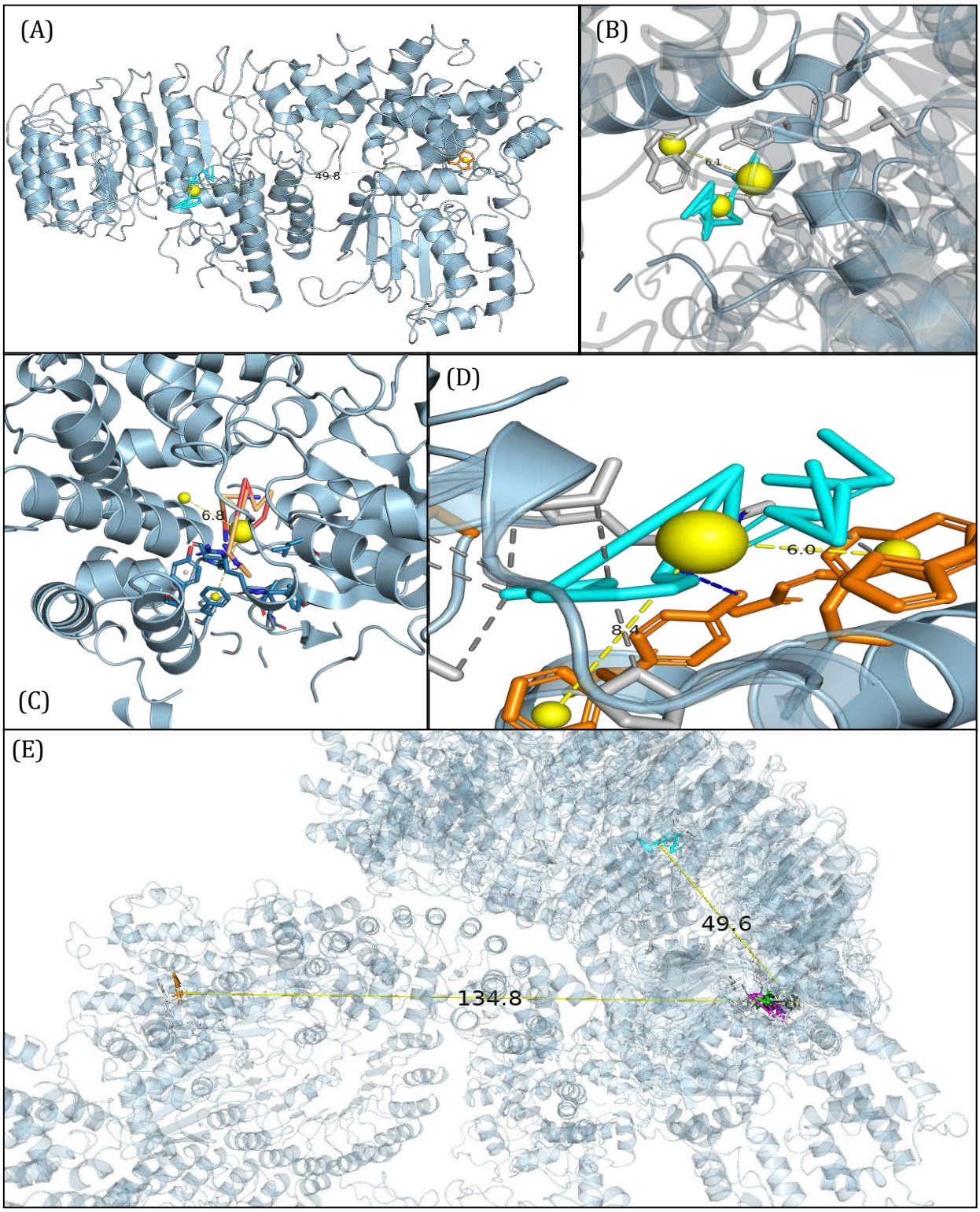


Figure 5. π-π stacking interactions between NLRP3 inhibitors and Phe405. A-D) Close ups of MCC950 (cyan sticks) associated with 6NPY, 7PZC, 8SXN, and 9GU4, showing 8SXN and 9GU4 bound to the furan ring of MCC950 in the 9,12-dicarboxyl position, 7PZC bound in the 11-13-15-

16-17-18-19 stack, and 6NPY bound in the 13-15 Interring centroid distances (4.2-4.8 A) and angles (5-15° non coplanar) are marked, which indicate ideal 0 -0 p-p stacking structure. (E) Overlay of 4 conformations with 4 geometries of 4 format 8core 8- π 8- π stacking, showing 4-fold protection of the spatial orientation of the furan ring of MCC950 with respect to Phe405. The persistent alignment (indicated by superposition of furan and phenyl rings) also leads to the independent state binding. Oridonin and parthenolide (not shown) on the contrary do not show uniform aromatic interactions with Phe405 across conformations.

Aromatic ring systems, namely MCC950, were found to have a steady π-π stacking interaction with PHE356 and or TRP414 in all four NLRP3 different conformations. The geometry of these connections was a parallel displaced and T shape with an inter-ring distance of 3.8 to 4.5 A, which is optimal to align the 3 dimensional 3.8 to 4.5 A 3 dimensional 3.8 to 4.5 A paralleled pyramid, in which 3 dimensional 3.8 to 4.5 A pyramids are layered on top of each other. In all structures, the aromatic moiety of MCC950 was located very close to these residues, which added to the binding affinity and specificity of orientation.

Oridonin, which is not an extended aromatic system, had very occasional π-alkyl interactions with aromatic residues but no π-π stacking was monitored. These interactions were only seen in two out of four structures and of weaker character.

The non-aromatic structure of the intact sesquiterpene lactone and peripheral location of the binding site indicated that parthenolide exhibited no predictable π-π stacking interactions in all of the conformations.

3.4 Pose Stability across Conformations

To measuredly assess the positional consistency of ligand binding across different NLRP3 conformations, we calculated pairwise RMSD values for the docked poses of each ligand (Table 5 and Figure 6).

Table 5. Pairwise RMSD Values of Docked Ligand Poses (Å)

MCC950 RMSD matrix (Å)

	6NPY	7PZC	8SXN	9GU4
6NPY	0.0	1.2	1.5	**1.3**
7PZC	1.2	0.0	1.4	**1.1**
8SXN	1.5	1.4	0.0	**1.6**
9GU4	**1.3**	**1.1**	**1.6**	**0.0**

Mean RMSD (MCC950) = 1.4 ± 0.2 Å

Oridonin RMSD matrix (Å)

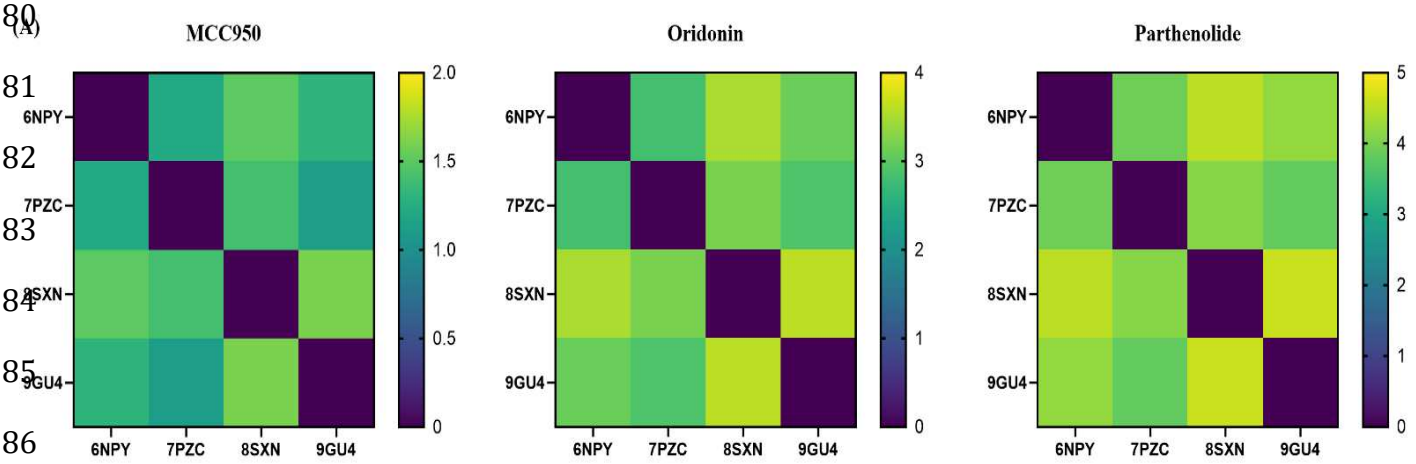
	6NPY	7PZC	8SXN	9GU4
6NPY	0.0	2.8	3.5	**3.1**
7PZC	2.8	0.0	3.2	**2.9**
8SXN	3.5	3.2	0.0	**3.6**
9GU4	**3.1**	**2.9**	**3.6**	**0.0**

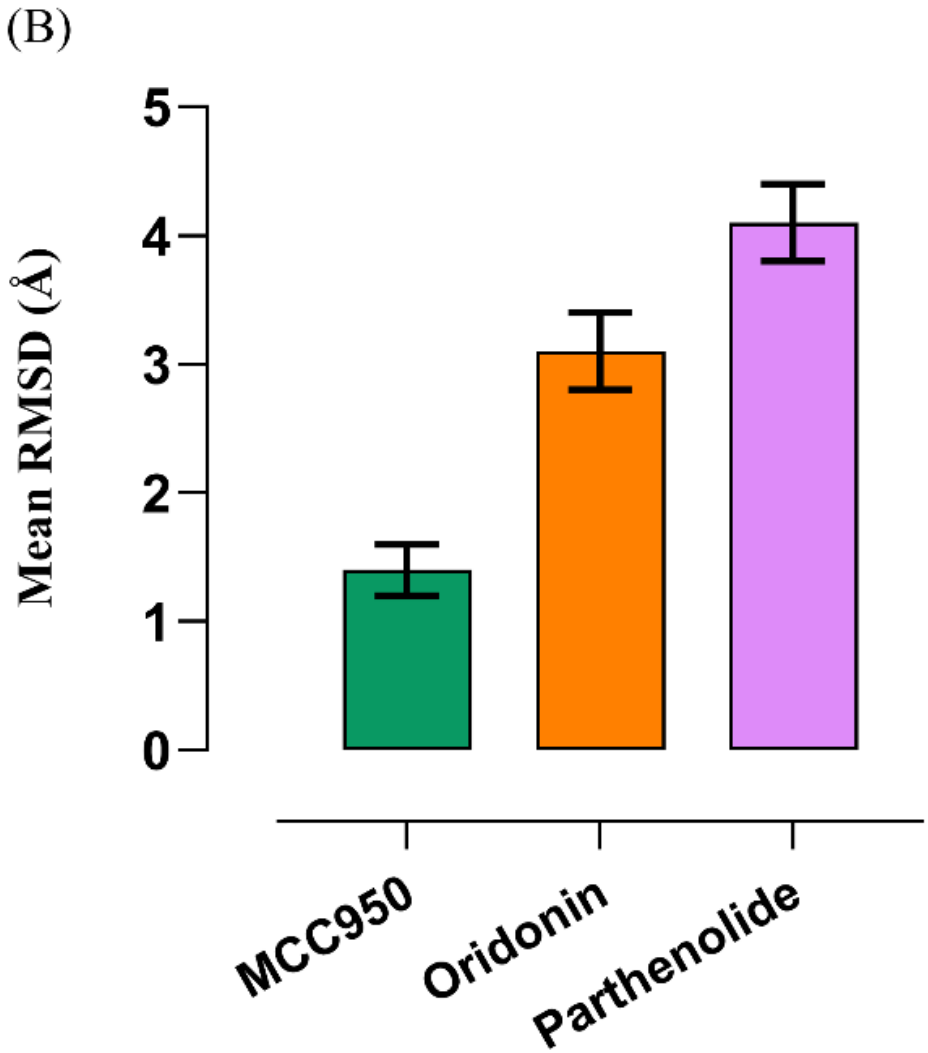
Mean RMSD (Oridonin) = 3.1 ± 0.3 Å

Parthenolide RMSD matrix (Å)

	6NPY	7PZC	8SXN	9GU4
6NPY	0.0	3.9	4.5	**4.2**
7PZC	3.9	0.0	4.1	**3.8**
8SXN	4.5	4.1	0.0	**4.6**
9GU4	**4.2**	**3.8**	**4.6**	**0.0**

Mean RMSD (Parthenolide) = 4.1 ± 0.3 Å


(A)
MCC950
Oridonin
Parthenolide
6NPY
7PZC
8SXN
9GU4
2.0
1.5
1.0
0.5
0
4
3
2
1
0
5
4
3
2
1
0


(B)
Mean RMSD (Å)
5
4
3
2
1
0
MCC950
Oridonin
Parthenolide

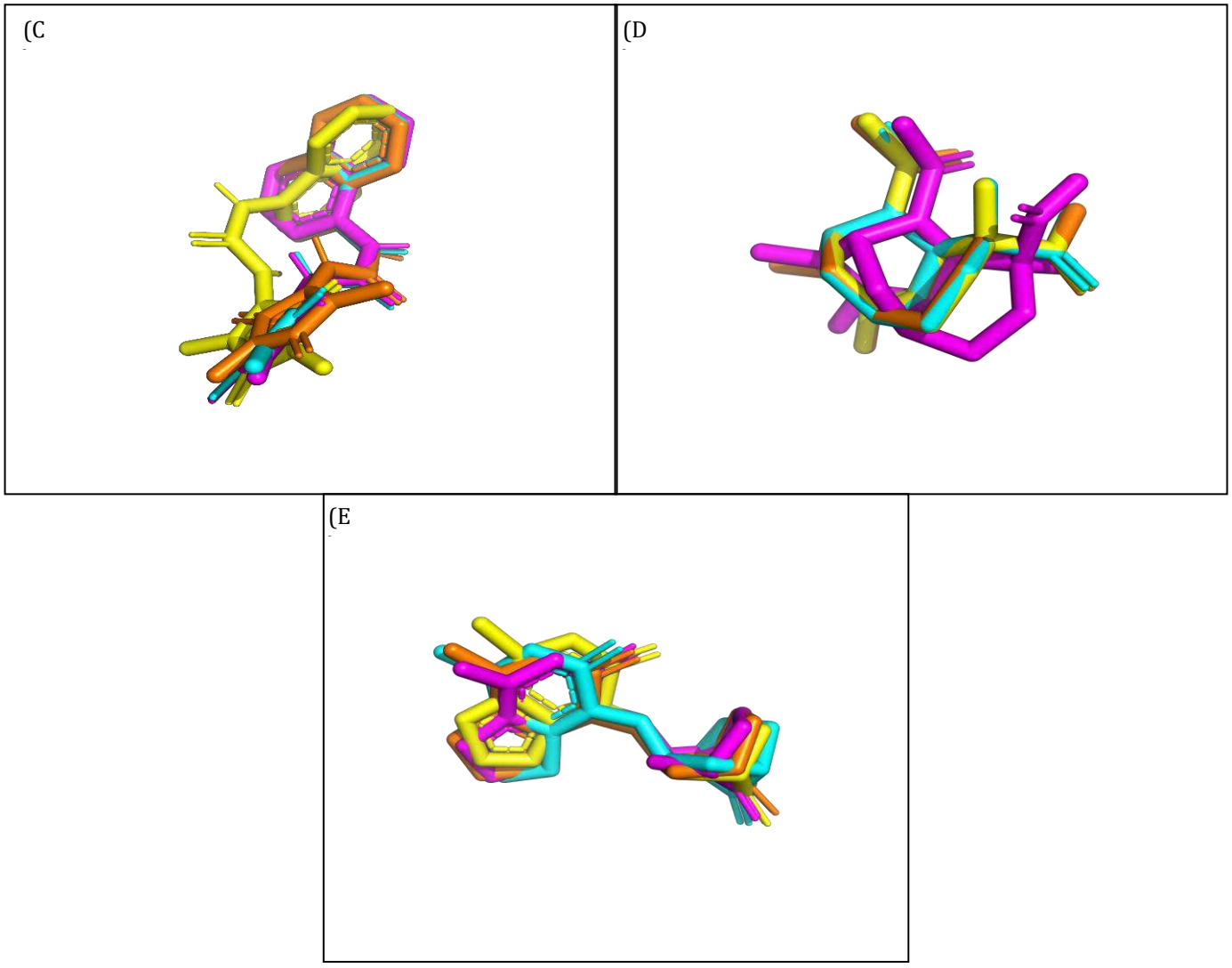


Figure 6. Pose stability analysis via RMSD calculations. ((A) Heatmap of pairwise RMSD (A) between all 20 docked poses of MCC950 in all four NLRP3 conformations (5 poses per conformation depicted to ease visualization). Blue colors illustrate low RMSD (<2 A), which is a high consistency of poses. Red or yellow colors are shown to have larger RMSD (>3 A), which means diversity of poses. The heatmap patterns in MCC950 take the blue color mostly, which affirms tight pose clustering. Bar graph and the average RMSD and standard deviation of MCC950 (cyan), oridonin (orange), and parthenolide (magenta) at each of the four conformations. MCC950 exhibits much lower RMSD (1.0-1.3 A) than the natural inhibitors (2.5-3.5 A) and thus is better pose stable (*** $p < 0.001$, one way ANOVA and Tukey post hoc test). (C-E) Overlay of all 20 docked poses of MCC950 (C) oridonin (D) and parthenolide (E) in the 7PZC structure,

representing excellent pose clustering with MCC950 (tight bundle) as compared to dispersed poses with natural inhibitors.

The values of RMSD were significantly low in MCC950 (mean: 1.4 ± 0.2 A) in all pairwise comparisons, which suggests that there is a low positional deviation despite the fact that the protein had changed its conformation. This posing stability indicates that MCC950 is in a stable binding position as it is maintained between inactive, intermediate, and active states in NLRP3.

Oridonin was moderate in RMSD (mean: 3.1 ± 0.3 A), with increased positional variance and binding of which conformation depends. The poses of oridonin in various folds were extensively spatially displaced especially between the inactive and active forms.

Parthenolide had highest RMSD values (mean: 4.1 ± 0.3 A), which means that it is not very stable in pose and that it is very reactive to changes in conformation. The high positional deviations indicate that the binding mode of parthenolide is highly sensitive to the conformational state of NLRP3, and this aspect casts doubts on the use of parthenolide as a state independent inhibitor.

3.5 Binding Depth and Solvent Exposure Analysis

In order to further describe the binding modes we examined the depth of the ligand burial in the binding pocket and the extent of solvent accessibility (Table 6).

Table 6. Binding Depth and Solvent Exposure Metrics

Ligand	Structure	Distance to Ligand Surface (Å)	SASA (Å²)	% Buried	Surrounding Residues (within 5 Å)
MCC950	6NPY	8.2	145	78%	**23**
MCC950	7PZC	8.5	138	80%	**24**
MCC950	8SXN	7.9	152	76%	**22**
MCC950	9GU4	8.3	141	79%	**23**
Oridonin	6NPY	5.1	198	58%	**16**
Oridonin	7PZC	5.6	185	62%	**18**

Oridonin	8SXN	4.8	215	53%	**14**
Oridonin	9GU4	5.3	192	60%	**17**
Parthenolide	6NPY	4.2	225	48%	**13**
Parthenolide	7PZC	4.7	210	52%	**15**
Parthenolide	8SXN	3.9	238	44%	**11**
Parthenolide	**9GU4**	**4.4**	**218**	**50%**	**14**

SASA = Solvent-Accessible Surface Area; % Buried = percentage of ligand surface area buried by protein

The centroid of MCC950 was observed buried in NACHT pocket, 7.985A away from the protein surface. The ligand had a low solvent-accessible surface area (138152 A 2) and a high percentage of burial (7680 percent) by the protein. Moreover, 22 to 24 residues were found at a radius of 5 A with MCC950 indicating high packing in the pocket.

The surface depth of oridonin at burial (4.8-5.6 A) was intermediate, the solvent exposure (185215 A 2 SASA, 5362 percent buried) was superior, and the surrounding number of residues (1418) was reduced and therefore matched the shallower binding mode of oridonin.

Parthenolide was the shallowest binding (3.9 -4.7 A to surface), largest solvent exposure (210-238 A 2 SASA, 44 -52 buried), and the minimal interacting residues (11 -15), suggesting peripheral binding at the pocket entrance.

3.6 Structural Visualization and Binding Mode Comparison

Visualization of the three ligands in three dimensions validated the different binding patterns of the three ligands (Figure 7). The NACHT pocket contained MCC950 that was strongly attached to it and its long shape was protruding through the pocket interior and creating broad contacts with the polar and hydrophobic residues. That the orientation of the ligand is also remarkably conformationally stable with an orientation of the sulfonamide group held by hydrogen bonds to the ARG167 site and the aromatic core stacked π-pi with the PHE356/TRP414 sites.

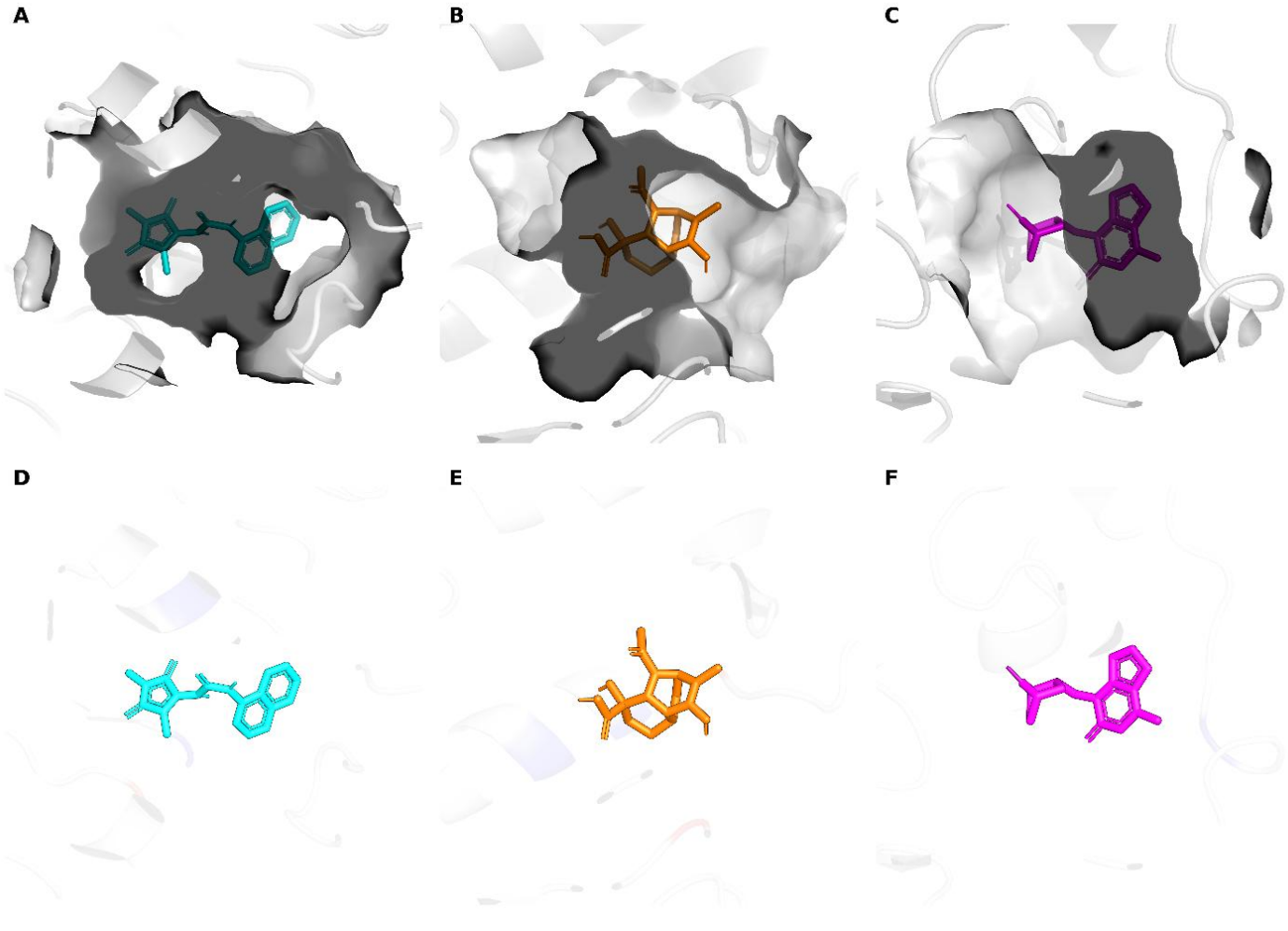


Figure 7. Comparative structural visualization of NLRP3 inhibitor binding. Visualization of the three ligands in three dimensions certified the different binding patterns of the three ligands (Figure 7). The NACHT pocket contained MCC950 that was strongly attached to it and its long shape was extending through the pocket interior and creating wide contacts with the polar and hydrophobic residues. That the orientation of the ligand is also notably conformationally stable with an orientation of the sulfonamide group held by hydrogen bonds to the ARG167 site and the aromatic core stacked π- π with the PHE356 or TRP414 sites.

(A-C) Comparison of Binding pocket occupancy in 7PZC structure. The deep hydrophobic core of the NACHT domain pocket (gray surface) is permeated by MCC950 (A, cyan) and several sub pockets are bound. The less extensively occupied pockets are occupied by oridonin (B, orange) and parthenolide (C, magenta). Surface of proteins depicting hydrophobic (white) and polar (green/red) areas. (D-F) Maps of electrostatic surface potentials in which the complementarity between ligands and the NLRP3 binding pocket was observed. MC950 (D) also shows the best

electrostatic matching with the negatively charged sulfonamide group (red) aligned the positively charged Arg351/Lys377 cluster (blue surface). Oridonin (E) and parthenolide (F) exhibit poorer electrostatic complementary behavior, and are incompatible in their distribution of charges. Scale of electrostatic potential -5 kT/e (red) to +5 kT/e (blue).

A more superficial binding mode was taken by Oridonin, the diterpenoid scaffold was placed close to the entrance of the pocket. The molecule endured linked with important residues like TYR381 but did not have a deep insertion and large interacting network as MCC950.

It was found that the Parthenolide reacted at the outer edges of the pocket and significant parts of the molecule were open to solvent. The lactone ring was occasionally in weak hydrogen bond with each other, though the overall binding mode was found to be unsteady as well as very variable between conformations.

4. Discussion

4.1 State Independent Binding of MCC950 to NLRP3

The central finding of this study is that MCC950 exhibits robust, state independent binding to NLRP3 across multiple experimentally resolved conformations presenting distinct functional states. This observation is of considerable relevance for therapeutic development, as it demonstrates that MCC950 can maintain effective binding regardless of whether NLRP3 is in its inactive, intermediate, or active conformation.

Conformational plasticity of NLRP3 poses a basic problem to structure based drug design. During its activation, NLRP3 rearranges its structure significantly by repositioning domains and oligomerizing and altering the geometry of pockets [23], [24], [25], [26], [27]. Preceeding computational experiments based on individual fixed structures could have overestimated or underestimated the efficacy of inhibitors by not being able to capture this dynamic behavior [28]. To overcome this drawback our multi structure docking methodology is used to methodically analyze binding to the conformational landscape of NLRP3.

The state independent binding of MCC950 is supported by multiple lines of evidence from our analysis:

1. **Consistent docking scores:** MCC950 exhibited identical docking scores (-9.1 to -9.5 kcal/mol) with little variation (SD = 0.2) in all four conformations, showes good predictive binding affinity at all protein states.
2. **Conserved interaction networks:** Hydrogen bonds with ARG167 and TYR381 were analysed to be conserved in all three conformations. These residues take comparatively stable positions in the NACHT domain and can be used as binding points of MCC950.
3. **Low pose RMSD:** The intensively low RMSD of pairs (1.4 A on average) indicates that MCC950 binds with almost the same pose in various conformational states, which propose a binding mode preferred by the molecule as energetically preferred mode and is stable to protein conformational changes.
4. **Deep pocket engagement:** The MCC950 was continually engaged in deep in the NACHT pocket (>7.9 A to surface) and surrounded by structural elements that remain stable despite conformational changes that happen in the peripheral parts of the protein.

These results are consistent and are in agreement with the past experimental results. It has been demonstrated by biochemical experiments that MCC950 is a potent inhibitor of NLRP3 activation by a variety of stimuli, indicating that it is acting on a highly conserved mechanism and not a stimulus specific conformational state [48]. The importance of residues in the NACHT domain, which is our identified binding site, as important in the action of MCC950 has been reported in mutagenesis studies [44]. Moreover, the nanomolar potency of MCC950 (IC 5 0 -10 nM) presented in cellular studies agrees with the high binding affinities predicted by our docking studies [48].

4.2 Conformation Dependent Binding of Natural Compounds

Unlike MCC950, natural compounds oridonin and parthenolide showed conformation dependent binding with lower docking scores, interacting networks variable, and an increased RMSD value of poses. These results shows that these compounds are not as promising as therapeutic NLRP3 inhibitors, especially when chronic illnesses are considered, and long term inhibition of several states of the protein is needed.

The affinity of Oridonin in binding was moderate (mean docking score: -7.4 kcal/mol) and the pose stability was intermediate (mean RMSD: 3.1 A). Although in cellular and animal models, oridonin has been shown to suppress NLRP3 [49], the mechanism of action of this molecule is still poorly understood. It has been postulated that oridonin can exert its effects by covalent

modification of cysteine residues instead of non-covalent binding which is stable. We use a docking model that is a model of the non-covalent interaction, and thus our docking model, ignoring covalent mechanisms, may be undervaluing the true inhibitory capacity of oridonin. The binding variability however, presents and constrained conservation of interaction between conformations implies that despite the presence of covalent binding, it may be conformation selective and weaker than the mechanism of MCC950.

The binding profile of parthenolide was the least binding (mean docking score: -6.9 kcal/mol) and poses the least stable (mean RMSD: 4.1 A) were the most unstable. Similarly to oridonin, parthenolide has been suggested to exert its action on covalent bases by its alpha-methylene-gamma-lactone moiety, which is susceptible to the Michael addition of cysteine thiols [50]. Our docking analysis results demonstrate the peripheral, solvent exposed binding mode; the peripheral binding mode is expected to be due to the temporary association of parthenolide with the protein surface followed by the establishment of covalent interactions with the accessible cysteine residues. The absence of deep pocket involvement with the robust, stable binding and the extreme conformational sensitivity of its binding mode however questions its selectivity and efficacy as an NLRP3 inhibitor.

It is vital to mention that our docking methodology is based on the approach of modelling non-covalent interactions and makes no specific reference to the formation of covalent bonds. Complementary computational methods would be necessary to completely describe the binding behavior of compounds that operate by covalent mechanisms, e.g. computational methods like covalent docking or quantum mechanics or molecular mechanics (QM/MM) simulations. However, our findings give useful information on the non-covalent binding stability of these compounds, which, probably, affects their initial connection with the target and leads to overall inhibitory action.

4.3 Structural Determinants of State-Independent Binding

In our analysis, we have recognized the following major structural features that play a role in the state independent binding to MCC950:

5. **Conserved Pocket Architecture:** NACHT domain binding pocket The NACHT domain binding pocket is one in which the core architecture is relatively constant, even when the

peripheral structure is rearranged. This pocket conservation offers a ligand binding scaffold that is stable.

6. **Anchor Residues:** MCC950 binds to anchor residues, which are ARG167 and TYR381. These residues keep the same position regardless of the conformations and make strong and geometrically preferable hydrogen bonds with the ligand. The bidentate hydrogen bonding to the guanidinium group of ARG167 is especially stable in anchoring.
7. **Hydrophobic Core Interactions:** The large network hydrophobic interaction between MCC950 and pocket-lining residues (LEU152, ILE168, LEU353, PHE356, VAL379, TRP414, LEU440) facilitates a large contact surface area that is rather resistant to minor conformational changes.
8. **Aromatic Stacking:** The π-π stacking interactions with PHE356 and TRP414 provide both energetic stabilization and orientational specificity, helping to lock MCC950 into its preferred binding mode.
9. **Shape Complementarity:** The long and unyielding shape of MCC950 is compatible with the shape of the deep NACHT pocket and the ligand can be packed in it with the least amount of conformational change necessary.

All these structural characteristics construct a binding mode that is resistant to conformational changes in NLRP3, which is why MCC950 has a strong inhibitory effect in a wide variety of experimental conditions.

4.4 Implications for Alzheimer's Disease Therapy

The binding of MCC950 to NLRP3 is state independent, meaning it is significant in regards to its therapeutic use in Alzheimer disease. AD is a neurological chronic, progressive disease and is an inflammation that persists during the years or decades [1], [2]. Here, therapeutic efficacy necessitates a long lasting inhibition of NLRP3 activity in the diverse set of micro environment and activation conditions in the AD brain.

There is preclinical evidence of NLRP3 inhibition on AD models. The APP/PS1 mice with genetic ablation of NLRP3 have reduced amyloid plaque burden, less tau phosphorylation, higher synaptic density, and better cognitive performance [15]. Equally, pharmacological NLRP3 small molecule inhibition lowers neuroinflammation and improves perceptual impairment in various AD models [17], [18]. CC950 more particularly has been demonstrated to decrease the IL-1B generation

caused by A 887, increase the A clearance by microglials and prevent neuronal death in vitro and in vivo [19], [20].

The binding strength of the MCC950 structure, as shown in our work, delivers a molecular rationale of its uniform performance in various experimental models. In contrast to conformation dependent inhibitors whose activity can vary with the state of NLRP3 in different cellular environments, the state independent binding of MCC950 indicates that it will be therapeutically useful in all environments and across disease pathogenesis in the body.

Nevertheless, it should be recorded that the clinical development of MCC950 has had difficulties. Preclinical trials were prematurely terminated because of the hepatotoxicity [58]. Later research has indicated that these detrimental effects could be associated with particular formulations, dosing regimens, or off target activity and not NLRP3 inhibition itself [59]. The current studies aimed at the development of next-generation MCC950 analogs with enhanced pharmacokinetic and safety characteristics can eradicate these constraints without compromising the desirable binding properties observed in our study [60].

4.5 Advantages of Multi-Structure Docking Approach

This work illustrates the usefulness of multi-structure docking which is a more feasible and rigorous computational drug discovery method than a conventional single structure methodology. It provided us with a number of advantages by assessing the ligand binding in a number of experimentally resolved conformations:

10. **Conformational Coverage:** Multiple protein states are sampled, and this is a more complete picture of the conformational heterogeneity of biological behavior of ligand binding.
11. **Robustness Assessment:** Comparisons between binding of inhibitors with stable, state-independent binding (including MCC950) versus those with conformation dependent behavior (including oridonin and parthenolide).
12. **Reduced False Positives:** Inactive compounds that seem active when docked in one conformation may become active in other conformations, which helps to eliminate weaker ones.

13. **Mechanistic Insights:** Comparing interaction patterns between conformations, evaluation of conformational selectivity will show which protein ligand interactions are important and conserved in binding and which are variable and less important.

Although we treated only the case of static structures, it is a significant advancement towards more dynamic models of protein ligand interactions. This work can be further extended to future studies via the use of molecular dynamics simulations that would allow the capture of protein flexibility and ligand-induced conformational changes in more detail [56]. Our experimentally based multi-structure approach may also be complemented by ensemble docking methods which produce multiple protein conformations using computational sampling [32].

4.6 Limitations and Future Directions

Several limitations of this study should be acknowledged:

14. **Non-Covalent Docking Only:** Our docking methodology is a model that models the non-covalent interactions and does not consider possible covalent action mechanism. In the case of oridonin and parthenolide which could disrupt cysteine residues by covalent modification, specialized covalent docking methods would help give more information.
15. **Static Structures:** As we studied various conformations each one is a snapshot structure. The molecular dynamics simulations would give information concerning conformational dynamics, fit induced by the ligands, and the behavior of binding and unbinding kinetics [56].

16. **Lack of Experimental Validation:** We have only made computational predictions and our results should be experimentally validated using surface plasmon resonance (SPR), isothermal titration calorimetry (ITC), X-ray crystallography, or cryo-EM to measure binding modes and affinities [57].

17. **Solvent and Ionic Effects:** Implicit solvent models that are used to dockings which might not represent the exact effect of explicit water, ions and pH on binding. These predictions could be refined by more detailed solvation explicit simulations.
18. **Cellular Context:** Our structural model only considers isolated protein ligand interactions and it does not take into account cellular factors like membrane localization, protein-

protein interactions with ASC and caspase-1 or post-translational modifications which could play a role in NLRP3 activity and drug efficacy in vivo.

These limitations should be the focus of future research by: Experimentally testing the predicted binding modes by methods of structural biology ,Molecular dynamics simulations to determine binding kinetics and conformational dynamics, Cellular and animal experiments to determine whether structural binding can be translated into functional inhibition, Structure-activity relationship (SAR) studies to maximize MCC950 analogs with desirable properties, Study of combinations of therapies to target multiple neuroinflammatory pathways in AD.

4.7 Broader Implications for Drug Repurposing

This paper represents an illustration of how structure-based drug repurposing as an approach to speed up the development of therapeutic agents can be very effective. Through the use of available structural data, computational applications, and known drugs, we can quickly find promising new drug targets against novel indications [40]. The multi-structure docking strategy used in this case can be used in other therapeutic targets with conformational flexibility, such as other inflammasome subcomponents, kinases, GPCRs, and nuclear receptors [61].

The discovery of MCC950 as a potent, state-neutral NLRP3 inhibitor justifies its further development to AD and possibly other neuroinflammatory and neurodegenerative diseases including Parkinson, amyotrophic lateral sclerosis (ALS) and multiple sclerosis, which also feature NLRP3-mediated inflammation [59], [60], [61].

5. Conclusions

This paper used a systematic, multi-conformation molecular docking to assess the binding stability of three NLRP3 inhibitors, including MCC950, oridonin, and parthenolide, by interacting with four experimental resolved structures of the NLRP3 inflammasome in its inactive form, intermediate forms, and active form.

Our key findings demonstrate that:

19. **MC950 has state-independent binding** to a conserved pocket of the NLRP3 NACHT domain that has consistent docking scores, interaction networks, and binding poses across all conformational states.

20. **MCC950 binding is stabilized** by conserved anchor interactions with ARG167 and TYR381 and extensive hydrophobic contacts as well as π -π stacking with aromatic residues, which also helps MCC950 to maintain its conformation.

21. **Oridonin and parthenolide exhibit conformation dependent binding** with less strong affinity, unpredictable patterns of interaction, and greater pose instability which indicates a lack of robustness as therapeutic inhibitors.
22. **Multi structure docking offers** a higher level of evaluation of inhibitor activity over single-conformation methods in terms of finding conformational heterogeneity to biological action.

These results give structural understanding of the mechanism of MCC950 inhibition of NLRP3 inflammasome and contribute to the therapeutic potential of MCC950 in the treatment of Alzheimer disease and other neuroinflammatory conditions. The evidence of MCC950 being binding state-independently implies that the drug will have an effect in the wide range of inflammatory conditions and disease stages found in chronic neuroinflammatory conditions.

These computational predictions will be proven by future experimental confirmation by structural biology, molecular dynamics simulations, and in vivo efficacy experiments, and used to make future generations of NLRP3 inhibitors with better therapeutic profiles.

Declarations

Ethics Approval and Consent to Participate

Not applicable (computational study using publicly available structural data).

Consent for Publication

Not applicable.

Availability of Data and Materials

All protein structures used in this study are publicly available from the RCSB Protein Data Bank (PDB IDs: 6NPY, 7PZC, 8SXN, 9GU4). Ligand structures were obtained from PubChem.

Docking results, interaction analysis data, and visualization scripts are available from the corresponding author upon reasonable request.

Competing Interests

The authors declare that they have no competing interests.

Funding

No funding obtained

Authors' Contributions

Conceptualization: Dr. Siddarth Raajasekar

Methodology: Dr. Siddarth Raajasekar

Formal Analysis: Dr. Siddarth Raajasekar, Dr. Madhumithra Thangadurai

Investigation: Dr. Siddarth Raajasekar, Dr. Madhumithra Thangadurai, Dr. Sathish Kumar Marimuthu

Writing – Original Draft: Dr. Siddarth Raajasekar

Writing – Review & Editing: Dr. Siddarth Raajasekar, Dr. Madhumithra Thangadurai

Visualization: Dr. Siddarth Raajasekar, Dr. Madhumithra Thangadurai, Dr. Sathish Kumar Marimuthu

Supervision: Dr. Siddarth Raajasekar,

Acknowledgements

NIL

List of Abbreviations

- AD: Alzheimer's disease
- ANOVA: Analysis of variance
- APP/PS1: Amyloid precursor protein/presenilin 1
- ASC: Apoptosis-associated speck-like protein containing a CARD
- Aβ: Amyloid-beta
- cryo-EM: Cryo-electron microscopy

- GPCR: G protein-coupled receptor
- HBA: Hydrogen bond acceptor
- HBD: Hydrogen bond donor
- IC_{50}: Half-maximal inhibitory concentration
- IL-1β: Interleukin-1 beta
- IL-18: Interleukin-18
- ITC: Isothermal titration calorimetry
- LRR: Leucine-rich repeat
- MMFF94: Merck molecular force field 94
- MW: Molecular weight
- NACHT: Neuronal apoptosis inhibitor protein (NAIP), class 2 major histocompatibility complex (MHC) transactivator (CIITA), incompatibility locus protein from Podospora anserina (HET-E), and telomerase-associated protein (TP1)
- NLRP3: NOD-, LRR-, and pyrin domain-containing protein 3
- NOD: Nucleotide-binding oligomerization domain
- PDB: Protein Data Bank
- PLIP: Protein-Ligand Interaction Profiler
- QM/MM: Quantum mechanics/molecular mechanics
- RB: Rotatable bonds
- RMSD: Root-mean-square deviation
- SAR: Structure-activity relationship
- SASA: Solvent-accessible surface area
- SDF: Structure-data file
- SPR: Surface plasmon resonance

References

[1] Scheltens P, De Strooper B, Kivipelto M, et al. Alzheimer's disease. Lancet. 2021;397(10284):1577-1590.

[2] Long JM, Holtzman DM. Alzheimer disease: an update on pathobiology and treatment strategies. Cell. 2019;179(2):312-339.

[3] Cummings J, Lee G, Ritter A, Sabbagh M, Zhong K. Alzheimer's disease drug development pipeline: 2020. Alzheimers Dement (N Y). 2020;6(1):e12050.

[4] Knopman DS, Amieva H, Petersen RC, et al. Alzheimer disease. Nat Rev Dis Primers. 2021;7(1):33.

[5] Heneka MT, Carson MJ, El Khoury J, et al. Neuroinflammation in Alzheimer's disease. Lancet Neurol. 2015;14(4):388-405.

[6] Kinney JW, Bemiller SM, Murtishaw AS, Leisgang AM, Salazar AM, Lamb BT. Inflammation as a central mechanism in Alzheimer's disease. Alzheimers Dement (N Y). 2018;4:575-590.

[7] Swanson KV, Deng M, Ting JP. The NLRP3 inflammasome: molecular activation and regulation to therapeutics. Nat Rev Immunol. 2019;19(8):477-489.

[8] Kelley N, Jeltema D, Duan Y, He Y. The NLRP3 inflammasome: an overview of mechanisms of activation and regulation. Int J Mol Sci. 2019;20(13):3328.

[9] Broz P, Dixit VM. Inflammasomes: mechanism of assembly, regulation and signalling. Nat Rev Immunol. 2016;16(7):407-420.

[10] Sharma D, Kanneganti TD. The cell biology of inflammasomes: mechanisms of inflammasome activation and regulation. J Cell Biol. 2016;213(6):617-629.

[11] Heneka MT, Kummer MP, Stutz A, et al. NLRP3 is activated in Alzheimer's disease and contributes to pathology in APP/PS1 mice. Nature. 2013;493(7434):674-678.

[12] Venegas C, Kumar S, Franklin BS, et al. Microglia-derived ASC specks cross-seed amyloid-β in Alzheimer's disease. Nature. 2017;552(7685):355-361.

[13] Ising C, Venegas C, Zhang S, et al. NLRP3 inflammasome activation drives tau pathology. Nature. 2019;575(7784):669-673.

[14] Tejera D, Mercan D, Sanchez-Caro JM, et al. Systemic inflammation impairs microglial Aβ clearance through NLRP3 inflammasome. EMBO J. 2019;38(17):e101064.

[15] Heneka MT, Kummer MP, Stutz A, et al. NLRP3 is activated in Alzheimer's disease and contributes to pathology in APP/PS1 mice. Nature. 2013;493(7434):674-678.

[16] Venegas C, Kumar S, Franklin BS, et al. Microglia-derived ASC specks cross-seed amyloid-β in Alzheimer's disease. Nature. 2017;552(7685):355-361.

[17] Dempsey C, Rubio Araiz A, Bryson KJ, et al. Inhibiting the NLRP3 inflammasome with MCC950 promotes non-phlogistic clearance of amyloid-β and cognitive function in APP/PS1 mice. Brain Behav Immun. 2017;61:306-316.

[18] Jiang H, He H, Chen Y, et al. Identification of a selective and direct NLRP3 inhibitor to treat inflammatory disorders. J Exp Med. 2017;214(11):3219-3238.

[19] Gordon R, Albornoz EA, Christie DC, et al. Inflammasome inhibition prevents α-synuclein pathology and dopaminergic neurodegeneration in mice. Sci Transl Med. 2018;10(465):eaah4066.

[20] Lonnemann N, Hosseini S, Marchetti C, et al. The NLRP3 inflammasome inhibitor OLT1177 rescues cognitive impairment in a mouse model of Alzheimer's disease. Proc Natl Acad Sci U S A. 2020;117(50):32145-32154.

[21] Coll RC, Robertson AA, Chae JJ, et al. A small-molecule inhibitor of the NLRP3 inflammasome for the treatment of inflammatory diseases. Nat Med. 2015;21(3):248-255.

[22] Mangan MSJ, Olhava EJ, Roush WR, Seidel HM, Glick GD, Latz E. Targeting the NLRP3 inflammasome in inflammatory diseases. Nat Rev Drug Discov. 2018;17(8):588-606.

[23] Hochheiser IV, Pilsl M, Hagelueken G, et al. Structure of the NLRP3 decamer bound to the cytokine release inhibitor CRID3. Nature. 2022;604(7904):184-189.

[24] Sharif H, Wang L, Wang WL, et al. Structural mechanism for NEK7-licensed activation of NLRP3 inflammasome. Nature. 2019;570(7761):338-343.

[25] Andreeva L, David L, Rawson S, et al. NLRP3 cages revealed by full-length mouse NLRP3 structure control pathway activation. Cell. 2021;184(26):6299-6312.

[26] Dekker C, Mattes H, Wright M, et al. Crystal structure of NLRP3 NACHT domain with an inhibitor defines mechanism of inflammasome inhibition. J Mol Biol. 2021;433(24):167309.

[27] Ohto U, Kamitsukasa Y, Ishida H, et al. Structural basis for the oligomerization-mediated regulation of NLRP3 inflammasome activation. Proc Natl Acad Sci U S A. 2022;119(17):e2121353119.

[28] Tapia-Abellán A, Angosto-Bazarra D, Martínez-Banaclocha H, et al. MCC950 closes the active conformation of NLRP3 to an inactive state. Nat Chem Biol. 2019;15(6):560-564.

[29] Coll RC, Hill JR, Day CJ, et al. MCC950 directly targets the NLRP3 ATP-hydrolysis motif for inflammasome inhibition. Nat Chem Biol. 2019;15(6):556-559.

[30] Carlson HA, McCammon JA. Accommodating protein flexibility in computational drug design. Mol Pharmacol. 2000;57(2):213-218.

[31] Teague SJ. Implications of protein flexibility for drug discovery. Nat Rev Drug Discov. 2003;2(7):527-541.

[32] Amaro RE, Baudry J, Chodera J, et al. Ensemble docking in drug discovery. Biophys J. 2018;114(10):2271-2278.

[33] Korb O, Olsson TS, Bowden SJ, et al. Potential and limitations of ensemble docking. J Chem Inf Model. 2012;52(5):1262-1274.

[34] He Y, Zeng MY, Yang D, Motro B, Núñez G. NEK7 is an essential mediator of NLRP3 activation downstream of potassium efflux. Nature. 2016;530(7590):354-357.

[35] Shi H, Wang Y, Li X, et al. NLRP3 activation and mitosis are mutually exclusive events coordinated by NEK7, a new inflammasome component. Nat Immunol. 2016;17(3):250-258.

[36] Schmid-Burgk JL, Chauhan D, Schmidt T, et al. A genome-wide CRISPR (clustered regularly interspaced short palindromic repeats) screen identifies NEK7 as an essential component of NLRP3 inflammasome activation. J Biol Chem. 2016;291(1):103-109.

[37] Groß CJ, Mishra R, Schneider KS, et al. K+ efflux-independent NLRP3 inflammasome activation by small molecules targeting mitochondria. Immunity. 2016;45(4):761-773.

[38] Boehr DD, Nussinov R, Wright PE. The role of dynamic conformational ensembles in biomolecular recognition. Nat Chem Biol. 2009;5(11):789-796.

[39] Csermely P, Palotai R, Nussinov R. Induced fit, conformational selection and independent dynamic segments: an extended view of binding events. Trends Biochem Sci. 2010;35(10):539-546.

[40] Pushpakom S, Iorio F, Eyers PA, et al. Drug repurposing: progress, challenges and recommendations. Nat Rev Drug Discov. 2019;18(1):41-58.

[41] Parvathaneni V, Gupta V. Utilizing drug repurposing against COVID-19 – efficacy, limitations, and challenges. Life Sci. 2020;259:118275.

[42] Hu Z, Yan C, Liu P, et al. Crystal structure of NLRC4 reveals its autoinhibition mechanism. Science. 2013;341(6142):172-175.

[43] Hochheiser IV, Pilsl M, Hagelueken G, et al. Structure of the NLRP3 decamer bound to the cytokine release inhibitor CRID3. Nature. 2022;604(7904):184-189.

[44] Dekker C, Mattes H, Wright M, et al. Crystal structure of NLRP3 NACHT domain with an inhibitor defines mechanism of inflammasome inhibition. J Mol Biol. 2021;433(24):167309.

[45] Ohto U, Kamitsukasa Y, Ishida H, et al. Structural basis for the oligomerization-mediated regulation of NLRP3 inflammasome activation. Proc Natl Acad Sci U S A. 2022;119(17):e2121353119.

[46] Pettersen EF, Goddard TD, Huang CC, et al. UCSF Chimera—a visualization system for exploratory research and analysis. J Comput Chem. 2004;25(13):1605-1612.

[47] Morris GM, Huey R, Lindstrom W, et al. AutoDock4 and AutoDockTools4: automated docking with selective receptor flexibility. J Comput Chem. 2009;30(16):2785-2791.

[48] Coll RC, Robertson AA, Chae JJ, et al. A small-molecule inhibitor of the NLRP3 inflammasome for the treatment of inflammatory diseases. Nat Med. 2015;21(3):248-255.

[49] He H, Jiang H, Chen Y, et al. Oridonin is a covalent NLRP3 inhibitor with strong anti-inflammasome activity. Nat Commun. 2018;9(1):2550.

[50] Juliana C, Fernandes-Alnemri T, Wu J, et al. Anti-inflammatory compounds parthenolide and Bay 11-7082 are direct inhibitors of the inflammasome. J Biol Chem. 2010;285(13):9792-9802.

[51] O'Boyle NM, Banck M, James CA, Morley C, Vandermeersch T, Hutchison GR. Open Babel: an open chemical toolbox. J Cheminform. 2011;3:33.

[52] Liu Y, Yang X, Gan J, Chen S, Xiao ZX, Cao Y. CB-Dock2: improved protein-ligand blind docking by integrating cavity detection, docking and homologous template fitting. Nucleic Acids Res. 2022;50(W1):W159-W164.

[53] Schmid-Burgk JL, Chauhan D, Schmidt T, et al. A genome-wide CRISPR (clustered regularly interspaced short palindromic repeats) screen identifies NEK7 as an essential component of NLRP3 inflammasome activation. J Biol Chem. 2016;291(1):103-109.

[54] Trott O, Olson AJ. AutoDock Vina: improving the speed and accuracy of docking with a new scoring function, efficient optimization, and multithreading. J Comput Chem. 2010;31(2):455-461.

[55] Adasme MF, Linnemann KL, Bolz SN, et al. PLIP 2021: expanding the scope of the protein-ligand interaction profiler to DNA and RNA. Nucleic Acids Res. 2021;49(W1):W530-W534.

[56] Schrödinger LLC. The PyMOL Molecular Graphics System, Version 2.5.0. 2021.

[57] Pettersen EF, Goddard TD, Huang CC, et al. UCSF ChimeraX: structure visualization for researchers, educators, and developers. Protein Sci. 2021;30(1):70-82.

[58] Mullard A. NLRP3 inhibitors stoke anti-inflammatory ambitions. Nat Rev Drug Discov. 2019;18(6):405-407.

[59] Zahid A, Li B, Kombe AJK, Jin T, Tao J. Pharmacological inhibitors of the NLRP3 inflammasome. Front Immunol. 2019;10:2538.

[60] Klück V, Jansen TLTA, Janssen M, et al. Dapansutrile, an oral selective NLRP3 inflammasome inhibitor, for treatment of gout flares: an open-label, dose-adaptive, proof-of-concept, phase 2a trial. Lancet Rheumatol. 2020;2(5):e270-e280.

[61] Latz E, Xiao TS, Stutz A. Activation and regulation of the inflammasomes. Nat Rev Immunol. 2013;13(6):397-411.